High-resolution structure of *myo*-inositol monophosphatase, the putative target of lithium therapy

Raj Gill, Fiyaz Mohammed, Rajji Badyal, Leighton Coates, Peter Erskine, Darren Thompson, Jonathan Cooper, Michael Gore and Stephen Wood*

Biomolecular Sciences Group, School of Biological Sciences, University of Southampton, Bassett Crescent East, Southampton SO16 7PX, England

Correspondence e-mail: steve@soton.ac.uk

Inositol monophosphatase is a key enzyme of the phosphatidylinositol signalling pathway and the putative target of the mood-stabilizing drug lithium. The crystal structure of bovine inositol monophosphatase has been determined at 1.4 Å resolution in complex with the physiological magnesium ion ligands. Three magnesium ions are octahedrally coordinated at the active site of each of the two subunits of the inositol monophosphatase dimer and a detailed three-metal mechanism is proposed. Ligands to the three metals include the side chains of Glu70, Asp90, Asp93 and Asp220, the backbone carbonyl group of Ile92 and several solvent molecules, including the proposed nucleophilic water molecule (W1) ligated by both Mg-1 and Mg-3. Modelling of the phosphate moiety of inositol monophosphate to superpose the axial phosphate O atoms onto three active-site water molecules orientates the phosphoester bond for in-line attack by the nucleophilic water which is activated by Thr95. Modelling of the pentacoordinate transition state suggests that the 6-OH group of the inositol moiety stabilizes the developing negative charge by hydrogen bonding to a phosphate O atom. Modelling of the post-reaction complex suggests a role for a second water molecule (W2) ligated by Mg-2 and Asp220 in protonating the departing inositolate. This second water molecule is absent in related structures in which lithium is bound at site 2, providing a rationale for enzyme inhibition by this simple monovalent cation. The higher resolution structural information on the active site of inositol monophosphatase will facilitate the design of substrate-based inhibitors and aid in the development of better therapeutic agents for bipolar disorder (manic depression).

1. Introduction

The discovery that lithium administration depletes brain inositol levels (Allison & Stewart, 1971) led to the formulation of the 'Inositol Depletion Hypothesis' whereby lithium was postulated to attenuate phosphatidyl inositol (PI) linked neurotransmitter receptor systems that are presumably overactive in mania (Berridge *et al.*, 1982). The maintenance and efficiency of these G-protein-coupled signalling systems depends crucially upon the resynthesis of the precursor lipid phosphatidyl inositol-3,4-diphosphate (PIP_2). Receptor-activated phospholipase C hydrolyzes PIP_2 to inositol 1,4,5-triphosphate (IP_3), which causes release of calcium from intracellular stores into the cytoplasm, and diacylglycerol (DAG), which activates protein kinase C. Generation of PIP_2 occurs either from the *de novo* biosynthesis of inositol from glucose-6-phosphate *via* L-inositol-1-phosphate [L-Ins(1)P; Eisenberg, 1967] or from the recycling of D-Ins(1)P generated

in PI-mediated signal transduction (Majerus *et al.*, 1988). In either case, the final hydrolysis of inositol monophosphate to inositol and inorganic phosphate (P_i) is catalyzed by *myo*-inositol monophosphatase (IMPase; EC 3.1.3.25; Chen & Charalampous, 1966), a homodimer of ∼30 kDa subunits which is activated by magnesium and specifically inhibited by therapeutic (0.5–1.5 m*M*) concentrations of lithium (Hallcher & Sherman, 1980). At concentrations above 5 m*M*, Mg^{2+}, like Li^+, becomes an uncompetitive inhibitor with respect to substrate (Leech *et al.*, 1993), indicating that both bind to the enzyme–substrate complex (Pollack *et al.*, 1993).

X-ray crystallographic studies by the Merck, Sharp and Dohme group (Bone *et al.*, 1992) have shown that the IMPase monomer consists of alternating layers of α-helices and β-sheet, forming a penta-layered αβαβα core structure which is also found in fructose 1,6-bisphosphatase (FBPase; Ke *et al.*, 1989), inositol polyphosphate 1-phosphatase (IPPase; York *et al.*, 1994), 3′-phosphoadenosine-5′-phosphatase (PAPase; Albert *et al.*, 2000) and 3′-phosphoadenosine-5′-phosphatase/inositol-1,4-bisphosphatase (PIPase; Patel, Yenush *et al.*, 2002), all of which are also Mg^{2+}-dependent and sensitive to Li^+ inhibition. The initial human IMPase structure was determined by multiple isomorphous replacement and the existence of only one inhibitory Gd^{3+} ion bound to Glu70, Asp90 and the carbonyl O atom of Ile92 (site 1) suggested that the high Li^+ concentration present in the crystallization conditions may have promoted Li^+ occupation of other metal sites. Subsequent structures of the inactive IMPase–Gd^{3+} structure in complex with Ins(1)P showed the phosphate moiety bound to the active-site metal and identified the roles of Asp93, Glu213 and the amide N atom of Ala196 in substrate binding (Bone, Frank, Springer, Pollack *et al.*, 1994). The structure of IMPase in complex with partially activating Mn^{2+} and phosphate identified two Mn^{2+} ions per IMPase subunit, one at site 1 and another adjacent at site 2 ligated to Asp90, Asp93, Asp220 and a phosphate O atom (Bone, Frank, Springer & Atack, 1994).

Early work suggested that IMPase operated by a two-metal mechanism. Equilibrium dialysis and binding studies with pyrene-maleimide-labelled bovine IMPase have shown that Mg^{2+} is required for phosphate binding and that at least two binding sites are present, one of high affinity and one of lower affinity (Greasley & Gore, 1993; Greasley *et al.*, 1994). Kinetic studies demonstrated that Mg^{2+} binding is cooperative and that this cooperativity is substrate-dependent (Ganzhorn & Chanal, 1990; Leech *et al.*, 1993; Strasser *et al.*, 1995), implying that the binding of Mg^{2+} must precede and also follow substrate binding. Equilibrium dialysis experiments yielded a K_d of ∼300 µ*M* for Mg^{2+} binding at the high-affinity site (site 1; Greasley & Gore, 1993) and fluorescence studies using pyrene-maleimide-labelled IMPase yielded a K_d of ∼3 m*M* for binding of Mg^{2+} at the low-affinity site (site 2; Greasley *et al.*, 1994). Additional indirect evidence for a two-metal mechanism came from the observation that both IPPase and FBPase hydrolyzed phosphate groups *via* a two-metal mechanism involving nucleophilic attack by water (York *et al.*, 1994; Zhang *et al.*, 1993).

Phosphate ^{18}O-ligand exchange occurs only in the presence of substrate, indicating that IMPase operates *via* a sequential ternary complex mechanism and that water attacks the phosphate ester bond directly (Leech *et al.*, 1993; Baker & Gani, 1991) in agreement with kinetic data, which show the absence of a phospho-enzyme intermediate (Ganzhorn & Chanal, 1990; Leech *et al.*, 1993). The Merck, Sharp and Dohme group used site-directed mutagenesis studies in conjunction with kinetic and molecular-modelling data to identify a water molecule (W1) coordinated by metal 1 and activated by Thr95 as the nucleophile (Pollack *et al.*, 1994). The mechanism would proceed *via* inline displacement with inversion of configuration at phosphate and the metal ion at site 2 was proposed to assist in phosphate coordination and charge stabilization during the transition state. In contrast, on the basis of kinetic data for the hydrolysis of different substrates, Gani and coworkers suggested that although metal 1 coordinates the phosphate moiety, it is metal 2 that activates a water molecule for nucleophilic attack on phosphorus (Cole & Gani, 1994; Wilkie *et al.*, 1995). In this proposal, the substrate 6-OH group hydrogen bonds to the nucleophile so that it is positioned for a non-inline attack on the phosphate P atom with adjacent displacement of the inositol moiety. Such a mechanism would proceed *via* an adjacent attack involving pseudo-rotation with retention of configuration. The recent determination of the stereochemical course of the reaction demonstrated that hydrolysis occurs with inversion at phosphorus (Fauroux *et al.*, 1999), indicating that the water nucleophile is indeed associated with metal 1. However, this interpretation excluded a role for the substrate 6-OH group which is essential for catalysis (Baker *et al.*, 1989, 1990, 1991). A new unified mechanism was proposed by Gani and co-workers in which the metal 2-bound water molecule (W2) serves as a proton donor for the inositolate leaving group and the 6-OH substrate group hydrogen bonds to this water to lower its pK_a value further for inline attack of the 1-inositolate anion (Miller *et al.*, 2000).

Because Li^+ competes uncompetitively with respect to the first Mg^{2+} ion required for high-affinity substrate binding (Hallcher & Sherman, 1980; Takimoto *et al.*, 1985), uncompetitively with respect to substrate (Gee *et al.*, 1988; Attwood *et al.*, 1988; Ganzhorn & Chanal, 1990) but competitively with respect to the second Mg^{2+} ion, it was proposed that Li^+ binds to the Mg^{2+}–IMPase ternary complex at metal site 2 (Gore *et al.*, 1993; Wilkie *et al.*, 1995) and prevents the dissociation of inorganic phosphate after hydrolysis (Shute *et al.*, 1988; Leech *et al.*, 1993; Pollack *et al.*, 1993; Cole & Gani, 1994; Villeret *et al.*, 1995; Atack *et al.*, 1995). A clue as to the mechanism of IMPase inhibition at high concentrations of Mg^{2+} comes from the finding that the Mg^{2+}-inhibition site is different from the Mg^{2+}-activation site (Ganzhorn & Chanal, 1990) and that both Li^+ and Mg^{2+} inhibit the enzyme uncompetitively through binding at the same site and through a similar mechanism (Hallcher & Sherman, 1980; Ganzhorn & Chanal, 1990; Leech *et al.*, 1993). The H217Q and C218A mutations in the proximity of site 2 eliminate not only the uncompetitive inhibition by Li^+ but also by Mg^{2+} (Gore *et al.*, 1993; Pollack *et al.*, 1993).

Table 1
Data-collection and refinement statistics for bovine IMPase.

Values in parentheses are for the outer shell.

Unit cell and symmetry	
Radiation source	ESRF (Grenoble) ID14-EH4
Radiation wavelength (Å)	0.979
Space group	$P1$
Unit-cell parameters	
a (Å)	47.2
b (Å)	55.2
c (Å)	60.9
α (°)	67.2
β (°)	69.6
γ (°)	85.1
Estimated solvent content (%)	46
Subunits in AU	2
Data set	
Resolution range† (Å)	27.1–1.40 (1.48–1.40)
Measured reflections	197109 (14822)
Unique reflections	89508 (7940)
R_{merge} (%)	10.0 (11.5)
Completeness (%)	84.7 (41.8)
$\langle I/\sigma(I)\rangle$	7.7 (7.7)
Multiplicity	2.2 (2.2)
Refinement statistics	
R factor (%)	15.26
R_{free} (%)	19.07
R.m.s.d. bond lengths (Å)	0.010
R.m.s.d. bond lengths (Å)	0.028
Residues in most favoured regions (%)	92.2
Residues in additionally allowed regions (%)	7.3
Mean B factors (Å^2)	
Protein main-chain atoms	14.61
Protein side-chain atoms	19.56
Water	27.13

† There are reflections between 1.40 and 1.24 Å resolution and these have been included in the refinement but not in the scaling statistics since the completeness in this resolution range is quite low. The data in this outer shell has an R_{merge} of 15.1% and a completeness of only 12.0%.

In addition, Tb^{3+} fluorescence quenching studies suggest that Li^+ binds at site 2 of IMPase (Pollack *et al.*, 1994) and Li^+ binding has been inferred at site 1 of FBPase (Villeret *et al.*, 1995), which corresponds to site 2 of IMPase.

Although the structure of IMPase in complex with Mn^{2+} and chloride had identified a third metal ion, which like the first metal ion was also ligated to Glu70, this was displaced upon phosphate binding and therefore dismissed as artifactual (Bone, Frank, Springer & Atack, 1994). Interestingly, the more recently determined structure of human IMPase in complex with Ca^{2+} and D-Ins1-P demonstrates retention of the third Ca^{2+} ion (Ganzhorn & Rondeau, 1997). Certain kinetic data have also been difficult to reconcile with a two-metal mechanism (Ganzhorn & Chanal, 1990; Strasser *et al.*, 1995; Ganzhorn *et al.*, 1996; Ganzhorn & Rondeau, 1997). More recently, the proposed two-metal mechanisms for FBPase and the archael FBPase/IMPases have been amended to three-metal mechanisms (Choe *et al.*, 1998; Johnson *et al.*, 2001).

The bovine IMPase structure presented here is the first IMPase structure to be solved in complex with the physiological Mg^{2+} ions. Three Mg^{2+} ions are bound at the active site and a detailed three-metal mechanism is proposed. The water nucleophile (W1) is now generated by the cooperative action of metals 1 and 3 and a second water molecule (W2) loosely

bound to metal 2 serves to neutralize the charge on the leaving inositolate. The role of the substrate 6-OH group is shown to be in the direct stabilization of the transition state and mechanisms are proposed for possible modes of Li^+ and Mg^{2+} inhibition.

2. Materials and methods

2.1. Protein expression and purification

Bovine IMPase was expressed in *Escherichia coli* strain BL21(DE3) following transformation with the pRSET5a plasmid (Diehl *et al.*, 1990). Cells were grown at 310 K with shaking to an absorbance of 0.9 (600 nm) in 4 l Luria Broth medium containing 50 µg ml^{-1} ampicillin. IPTG was then added to 0.4 mM and incubation continued for 12 h. All subsequent steps were performed at 277 K except where noted. Cells were pelleted (1800g for 30 min) and lysed by sonication in 30 ml buffer A (30 mM Tris–HCl pH 8.0, 0.1 mM EGTA, 0.1 mg ml^{-1} lysozyme, 0.1 mg ml^{-1} DNAse I). After centrifugation (40 000g for 30 min), the supernatant was decanted and heat-treated at 338 K for 1 h and the precipitated protein pelleted by centrifugation at 12 000g for 30 min. The supernatant was decanted and loaded onto a Q-Sepharose anion-exchange column pre-equilibrated in buffer B (30 mM Tris–HCl pH 8.0, 30 mM NaCl). Bound protein was eluted using a linear gradient of 0–100% buffer C (30 mM Tris–HCl pH 8.0, 300 mM NaCl). The active fractions were pooled and concentrated by 80% ammonium sulfate precpitation. The pellet was resuspended in 1 ml dialysis buffer (50 mM Tris–HCl pH 8.0, 20 mM EDTA, 1 mM EGTA, 0.7 mM 1,10-phenanthroline) and buffer-exchanged three times against 4 l dialysis buffer. Finally, the protein was dialyzed against 50 mM Tris–HCl pH 8.0.

2.2. Protein crystallization

Bovine IMPase was crystallized at room temperature using the vapour-diffusion method. Hanging drops were obtained by mixing equal volumes (2 µl) of protein solution (at a concentration of 20 mg ml^{-1} bovine IMPase in 20 mM Tris–HCl pH 7.5 containing 20 mM $MgCl_2$) with reservoir solution (0.1 M sodium acetate, 0.1 M sodium HEPES pH 8.5 and 15% PEG 4000).

2.3. X-ray data collection and processing

A single bovine IMPase crystal ($0.6 \times 0.4 \times 0.1$ mm) was transferred from 0 to 30%(v/v) glycerol in steps of 7.5% prior to flash-cooling in liquid ethane for cryo data collection. X-ray diffraction data were collected on beamline ID14-EH4 ($\lambda = 0.979$ Å) at the ESRF (Grenoble, France) using a Quantum 4 charge-coupled device detector (ADSC) with the crystal cooled at 100 K using a Cryostream (Oxford Cryosystems Ltd). The crystal diffracted X-rays to a resolution of 1.24 Å and was found to have crystallized in the triclinic space group $P1$ (unit-cell parameters $a = 47.2$, $b = 55.2$, $c = 60.9$ Å, $\alpha = 67.2$, $\beta = 69.6$, $\gamma = 85.1°$). The high-resolution and low-resolution passes consisted of collecting 180 1° and 60 3°

oscillation frames, respectively. The intensity data were processed with *MOSFLM* (Leslie, 1992) and reduced using programs from the *CCP*4 (Collaborative Computational Project, Number 4, 1994) suite.

2.4. Structure determination and refinement

The calculated crystal-packing parameter V_M assuming two bovine IMPase subunits (60 112 Da) per asymmetric unit is 2.28 $\text{Å}^3\text{ Da}^{-1}$, corresponding to a solvent content of 46% (Matthews, 1968). The structure of bovine IMPase was solved by molecular replacement using *AMoRe* (Navaza, 1994). The search model consisted of the human IMPase dimer (PDB code 2hhm) refined to 2.1 Å resolution, with the Gd^{3+} and SO_4^{2-} ions and all water molecules omitted. The cross-rotation calculations performed with a sphere of integration of 30 Å generated a strong rotation-function peak of 10σ ($\alpha = 205.82$, $\beta = 13.00$, $\gamma = 54.95°$), the next peak being 5.3σ above the background. The crystal packing of this solution was viewed using *MOLPACK* (Wang *et al.*, 1991) and displayed sensible crystal contacts.

The progress of refinement was verified by monitoring the variation of the free R factor (R_{free}) calculated from a test set of reflections (5% of data) which were set aside for cross-validation purposes (Brünger, 1992). The refinement of the molecular model was performed with *CNS* (Brünger *et al.*, 1998) using 67 643 reflections within the resolution range 20–1.24 Å. The initial round of refinement consisted of rigid-body refinement, positional refinement and individual isotropic B-factor refinement. Following the first round of refinement, the refined molecular model was used to calculate σ_A-weighted electron-density maps. Examination of these maps using *QUANTA* (Molecular Simulations Inc., Burlington, MA, USA) revealed well defined $F_o - F_c$ density for the side chains of bovine IMPase, allowing model rebuilding to take place. Following the first phase of manual building, the model was subsequently subjected to several alternating cycles of refinement and model building.

Once the R factor (and the R_{free}) had dropped below 30%, water molecules were placed at stereochemically acceptable sites following visual verification of the $2F_o - F_c$ map. Water molecules were only accepted if they appeared in $F_o - F_c$ maps contoured at 3σ, reappeared in subsequent $2F_o - F_c$ maps, formed hydrogen bonds with chemically reasonable groups and had B factors less than 50 Å^2. These water molecules were added in successive steps and were included in the subsequent refinement cycles.

Once isotropic refinement with *CNS* had converged ($R_{\text{factor}} = 18.7\%$, $R_{\text{free}} = 20.7\%$), an anisotropic description of the atomic displacements was introduced with the program *SHELX*97 (Sheldrick & Schneider, 1997). The molecular model was subjected to ten cycles of isotropic conjugate-gradient least-squares refinement (CGLS). In the subsequent refinement step riding H atoms were used, which further reduced both the R factor and R_{free} by 1%. The improved phase estimates substantially improved the quality of the electron-density maps, allowing the modelling of missing atoms and dual side-chain conformations. The final model was refined anisotropically, resulting in an appreciable drop in the R factor (15.3%) and R_{free} (19.1%). The reduction in both the R factor and R_{free} by 3.4 and 1.6%, respectively, unambiguously demonstrated that the anisotropic refinement was meaningful. Structures were depicted with *MOLSCRIPT* (Kraulis, 1991) and rendered with *RASTER3D* (Merritt & Bacon, 1997).

3. Results

3.1. Quality of the model

Bovine IMPase crystallized in space group $P1$ with a dimer (subunits A and B) in the unit cell. The structure was determined by molecular replacement using the struc-

Figure 1
(*a*) An example of the quality of the electron density at the active site allowing unambiguous modelling of the magnesium and water structure. The map was contoured at 1.5σ. (*b*) The active site of bovine IMPase depicting the octahedral coordination of each magnesium ion (distances in Å). Magnesium ions are depicted in purple and water molecules are depicted in red, light blue, orange and pink according to the revised three-metal mechanism proposed in §3.8.

ture of the human IMPase dimer as the search model and refined at 1.4 Å resolution to a final R factor of 15.3% (R_{free} of 19.1%). The final model consists of 4164 protein atoms, six Mg^{2+} ions and 518 water molecules. Inspection of the Ramachandran plot calculated with *PROCHECK* (Laskowski *et al.*, 1993) demonstrated that all residue main-chain dihedral angles reside in allowed regions, with 92.2% of residues residing in the most favourable region. The remaining residues reside in the additionally (7.3%) and generously (0.4%) allowed regions. The overall stereochemistry of the atomic model is good, with r.m.s. deviations from ideality for bond lengths and bond-angle distances of 0.01 and 0.03 Å, respectively. The data-collection and refinement statistics are presented in Table 1.

The quality of the final electron-density map is excellent for almost all residues in both subunits (Fig. 1a), with the exception of a few residues at the N- and C-termini. These residues are also highly disordered in all human IMPase structures. Several side-chain atoms were set to zero occupancy because either there was no visible electron density or the electron-density maps were too ambiguous to allow their placement. These discretely disordered residues are widely distributed over the surface of the molecule. In addition, there are several side chains that were assigned alternate conformations in each subunit (Thr14, Met34 and Val99 in subunit *A*, and Met31, Ser57, Gln147, Ser177 and Arg261 in subunit *B*).

3.2. Overall structure

As expected from their close sequence identity (85%), the overall fold of bovine IMPase is very similar to that of human IMPase, with each subunit being composed of nine α-helices and 13 β-strands that make up a penta-layered $\alpha\beta\alpha\beta\alpha$ sandwich (Fig. 2). The first layer consists of two antiparallel six- and five-turn α-helices (α_1, Trp5–Ala26; α_2, Ala44–Tyr62) connected by a β-hairpin (β_1, Asn32–Lys36; β_2, Asp41–Val43). The second layer is a large six-stranded antiparallel β-sheet (β_3, Ser66–Glu70; β_4, Pro85–Asp90; β_5, Val105–Val113; β_6, Lys116–Ser124; β_7, Asp128–Lys135; β_8, Lys137–Asn142) orientated parallel to the first α-helical layer. Also present in the second layer is a two-turn α-helical segment following strand β_3 (α_3, Glu70–Ala75) and a β-bulge (Asp90–Asp93) which extends into another two-turn α-helix (α_4, Thr95–Gly101). The third layer is composed of two three-turn parallel α-helices (α_7, Thr195–Ala205; α_8, Cys218–Glu230) aligned perpendicular to the second layered β-sheet. The fourth layer is made up of a five-stranded β-sheet [β_{10} (His188–Arg191) β_9, (Ser157–Thr161), β_{11} (Asp209–Gly215)

and β_{12} (Val234–Leu236) are oriented parallel, while β_{13} (Arg248–Ser254), positioned between strands β_{11} and β_{12}, is orientated antiparallel. The fourth layer also contains a one-turn α-helical segment preceding strand β_9 (α_5, Asn153–Ser157). Finally, the fifth layer is comprised of two antiparallel three and four-turn helices (α_9, Asn255–Ile266; α_6, Thr168–Cys184) that pack against the β-sheet of the fourth layer.

3.3. Comparison of bovine IMPase subunits *A* and *B*

There are no major differences between the two subunits, which superimpose with an r.m.s. deviation of 0.20 Å over 274 equivalent C^α atoms. With the exception of the C-terminus, the regions having the largest structural difference between the two subunits include the β-hairpin in the first layer (β_1 and β_2), helices α_2 and α_3, the following loop region and finally the N-terminal of helix α_6. These structural differences are also reflected in the average main-chain temperature factors. There are four regions with significantly higher B factors than the mean temperature factor, namely β_1 and the preceding loop, helix α_3 and the following loop region, the loop connecting strands β_{12} and β_{13} and the C-terminus, reflecting the mobility of the protein tail. The β-hairpin (Asn32–Val43) of subunit *B* is very mobile and associated with poor electron density. The
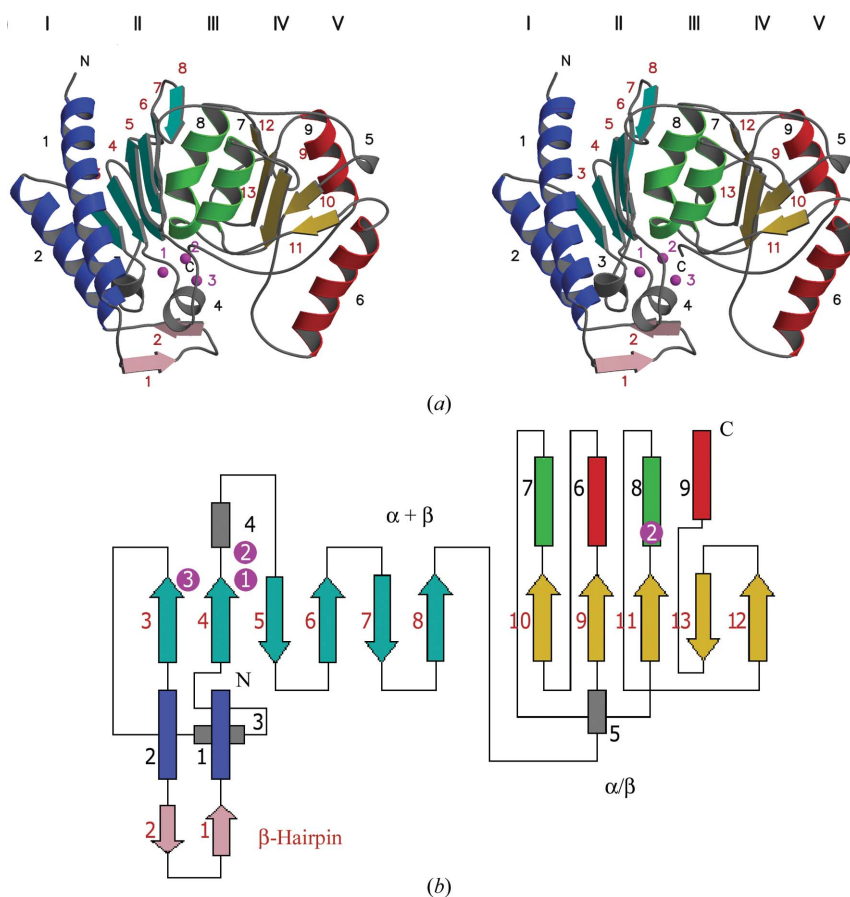

Figure 2
(*a*) A ribbon diagram of the overall fold of bovine IMPase depicting the penta-layered sandwich. α-Helices and β-sheets are labelled in black and red, respectively, and Mg atoms are depicted as purple spheres. (*b*) A topology diagram of bovine IMPase with each layer of secondary structure coloured differently.

equivalent region in subunit A is less disordered because it forms significantly more hydrophobic crystal contacts with a neighbouring molecule. The loop connecting strands β_{12} and β_{13} is also more disordered in subunit B than in subunit A owing to less extensive crystal contacts.

3.4. Comparison of bovine IMPase with human IMPase

The r.m.s. deviations between the structures of bovine IMPase and the highest resolution (2.1 Å) human IMPase structure are 0.64 Å for subunit A and 0.60 Å for subunit B, respectively, over 271 equivalent C^α atoms. The greatest differences are in the first layer of secondary structure ($\alpha_1\beta_1\beta_2\alpha_2$); if this region is discounted, the r.m.s. deviations decrease to 0.50 and 0.45 Å, respectively, over 210 equivalent C^α atoms. The conformational difference in the β-hairpin is consistent between bovine IMPase and all metal-bound human IMPase structures and may be attributed to the different packing in the crystal. In both bovine and human IMPase structures strand β_1 is not involved in crystal contacts, but there are multiple crystal contacts in strand β_2 of the bovine monomer, whereas the corresponding contacts for the human monomer are limited to Met34 and Leu35.

The bovine IMPase structure displays a lower average temperature factor (14.32 Å^2) than the human IMPase structure (25.09 Å^2) in accordance with its higher resolution. In both the human and bovine IMPase structures residues 74–85 (α_3) make no packing contacts in the crystal and possess high B factors. Residues 52–66 (α_2) also possess high B factors in the human IMPase structure but are involved in a lattice contact in the bovine IMPase structure. Of the 31 sequence differences between the bovine and human structures, half are compensatory substitutions that maintain hydrophobic contacts in the core of the structure (residues 33Ile/Val, 35Val/Leu, 40Ala/Val, 112Val/Ala, 117Met/Ile, 121Ile/Val, 126Leu/Val, 174Ile/Met, 175Ile/Val, 179Ile/Met, 183Leu/Phe, 185Leu/Ile, 187Ile/Val, 198Leu/Val, 236Leu/Met and 268Ile/Val). Other conservative substitutions include 133Gly/Ala, 207Ala/Gly and the substitutions 17Gly/Arg and 257Thr/Ile which are on the surface of the molecule. Two substitutions contribute to the maintenance of two hydrogen bonds in both structures (56Thr/Ser and 254Ser/Asn), four substitutions contribute to the gain of six hydrogen bonds and a salt bridge in bovine IMPase (24Arg/Cys, 128Asp/Gly, 181Arg/Lys and 253Ser/Ala) and three substitutions contribute to the gain of five hydrogen bonds in human IMPase (101Gly/Arg, 192Gly/Ser and 205Ala/Thr). The net gain of one hydrogen bond in the bovine structure is compensated for by the presence of Arg24, which prevents formation of the 24–125 disulfide bridge present in some human structures. This disulfide may stabilize layers 1 and 2 of the penta-layered structure which are located slightly closer to the body of the human structure,
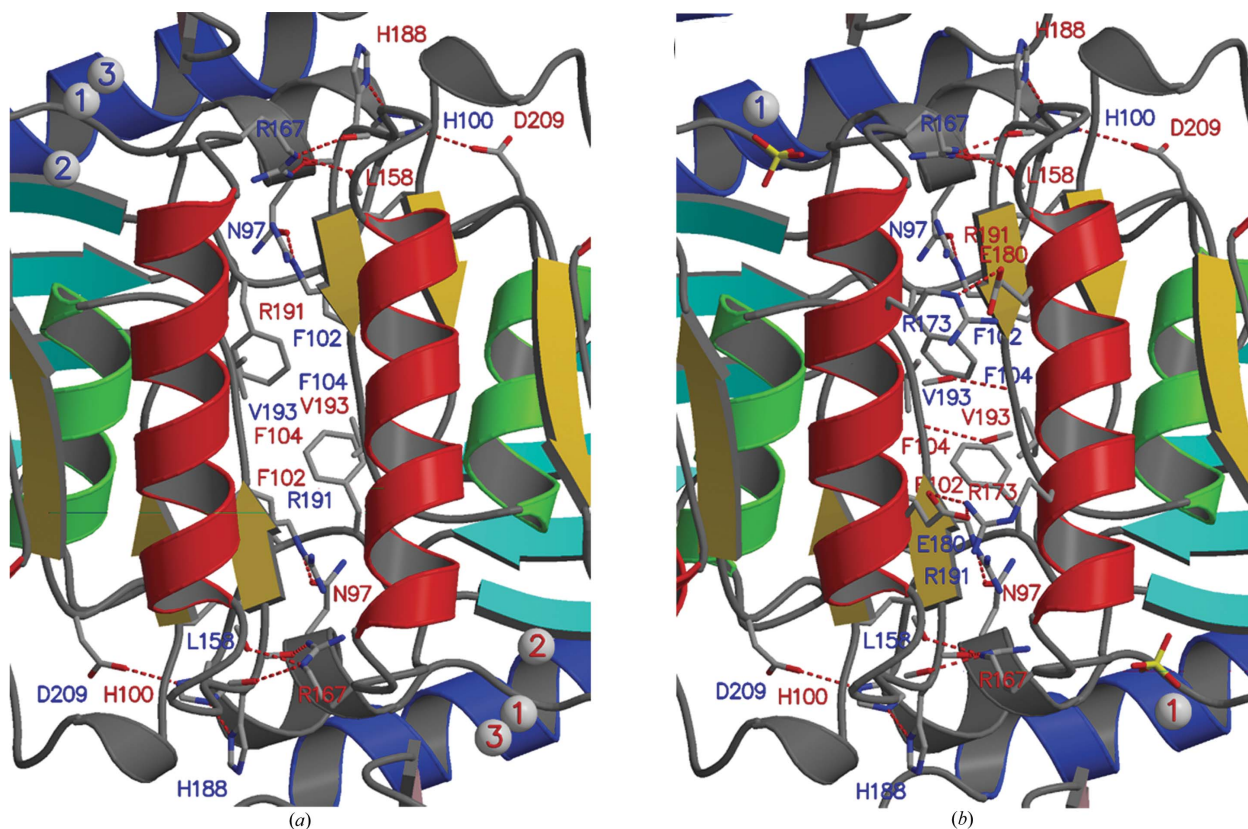

Figure 3
The dimer interface of (a) bovine IMPase and (b) human IMPase, displaying the hydrophobic and ionic interactions (subunit A labels in red and subunit B labels in blue).

although it may be artifactual since Cys24 is not evolutionarily conserved and IMPase is not an extracellular protein.

3.5. Comparison of the dimer interfaces of bovine IMPase and human IMPase

A comparison of the dimer interfaces of bovine and human IMPase (Fig. 3) is of interest as the non-polar α-hydroxy-phosphonate inhibitors (MacLeod *et al.*, 1992), which have high bioavailability in the brain and are more potent inhibitors of the bovine enzyme compared with the human enzyme, have been proposed to bind there (Ganzhorn *et al.*, 1998). Molecular modelling suggests that the hydrophobic part of the inhibitor interacts with residues 175–185, which have only 55% sequence identity between the human and bovine isozymes, and studies on the F183L human IMPase mutant implicate this residue as a major determinant for inhibitor specificity (Ganzhorn *et al.*, 1998)

The dimer interface of bovine IMPase is extensive (2296 Å^2), with the α_6 residues of both subunits making the major contacts (the primary sequence identity between human and bovine enzymes is only 66% for this α-helix). Since the dimer is formed *via* an approximate twofold axis in the crystal, not all contacts in the interface are duplicated. The interface has a more hydrophobic character than polar, with principal dimerization contacts involving several hydrophobic clusters. In the largest cluster, residues involved in these interactions include Phe102, Pro103, Phe104, Leu158, Val193 and the aliphatic moieties of His100 and Arg191. The hydrophobic contacts made between the bovine IMPase subunits are fewer when compared with the human IMPase interface. This is owing to the presence of smaller residues (Ala40 and Gly192 in bovine IMPase have replaced Val40 and Ser192 in human IMPase) and a compensatory hydrophobic residue exchange (Leu183 in bovine IMPase has replaced Phe183 in human IMPase) at the interface of the bovine dimer.

The dimer interface of bovine IMPase is further stabilized by two salt bridges (between His100 and Asp209 and between Arg173 and Glu180), five hydrogen bonds and a network of water molecules that make contact with both subunits. The side-chain O atom of Asn97 forms hydrogen bonds with the NE and NH2 atoms of Arg191, and the NE and NH2 atoms of Arg167 form hydrogen bonds with the carbonyl groups of Ile187 and His188. The latter also forms a hydrogen bond with His100. By contrast, in addition to the above interactions, the human interface is stabilized by three additional hydrogen bonds. Arg167 NE is within hydrogen-bonding distance of the carbonyl group of Phe183, whilst both carboxyl O atoms of Glu180 interact with Arg193 rather than just the one. Finally, the carbonyl group of Ser192 forms a hydrogen bond with the backbone amide of the same residue in the opposing monomer, whereas conformational differences mean that this does not apply for Gly192 in the bovine IMPase dimer.

3.6. The active site of bovine IMPase

The active site of bovine IMPase is located at the intersection of several secondary-structure elements (α_2, β_3, α_8 and residues 90–95, of which residues 90–93 form a β-bulge). Each subunit possesses three Mg^{2+}-binding sites in a hydrophilic cavity near the surface of the molecule. Several ordered water molecules in the active site serve as metal ligands and perform a structural role by forming hydrogen bonds to residues that make up the active site (Fig. 1*b*). The metal-binding sites were identified on the basis of three criteria. Firstly, $F_o - F_c$ maps calculated at 1.4 Å displayed clear peaks ranging from 5 to 10σ. Secondly, the coordination sphere of each metal site consisted of water molecules and carboxylate groups all within the accepted range for Mg^{2+}–oxygen distances. Thirdly, the coordination sphere of all three metal sites refined to octahedral geometry, consistent with the expected coordination for Mg^{2+}. All three Mg^{2+} ions displayed low temperature factors ranging from 6 to 20 Å^2, with the magnesium ion at site 3 displaying the highest thermal parameters, presumably because of its weak interaction with a single protein ligand; it is likely that this site is only occupied at higher Mg^{2+} concentrations.

The coordination sphere of Mg^{2+} at site 1 (Mg-1) consists of the conserved residues Glu70, Asp90, Ile92 and three water molecules. Mg-1 can be directly superposed onto the Gd-1,
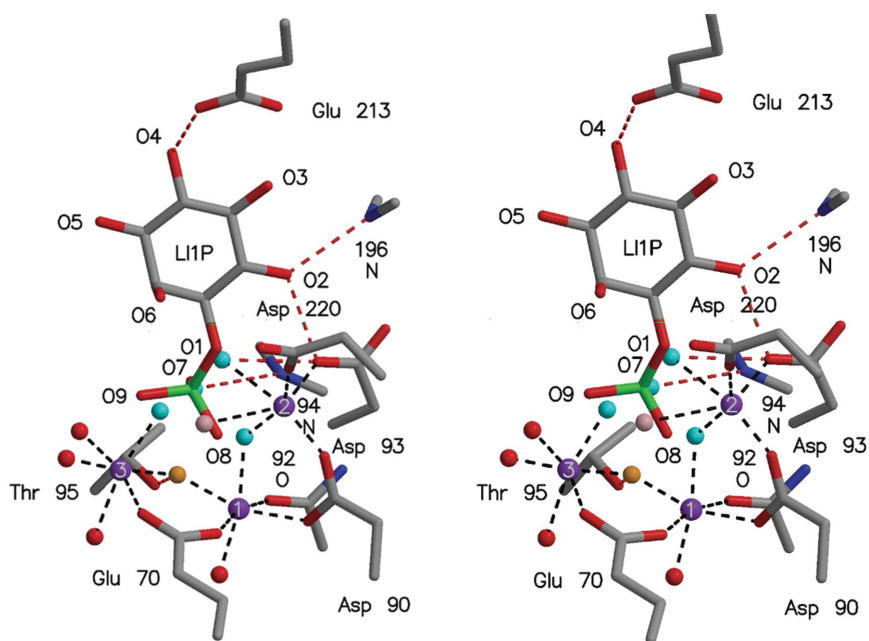

Figure 4
Superposition of L-Ins(1)P from the human IMPase–Gd^{3+}–L-Ins(1)P structure (Bone, Frank, Springer & Atack, 1994) at the active site of bovine IMPase. Water molecules displaced by O1 and the axial phosphate O atoms upon binding of the phosphate moiety are depicted in light blue.
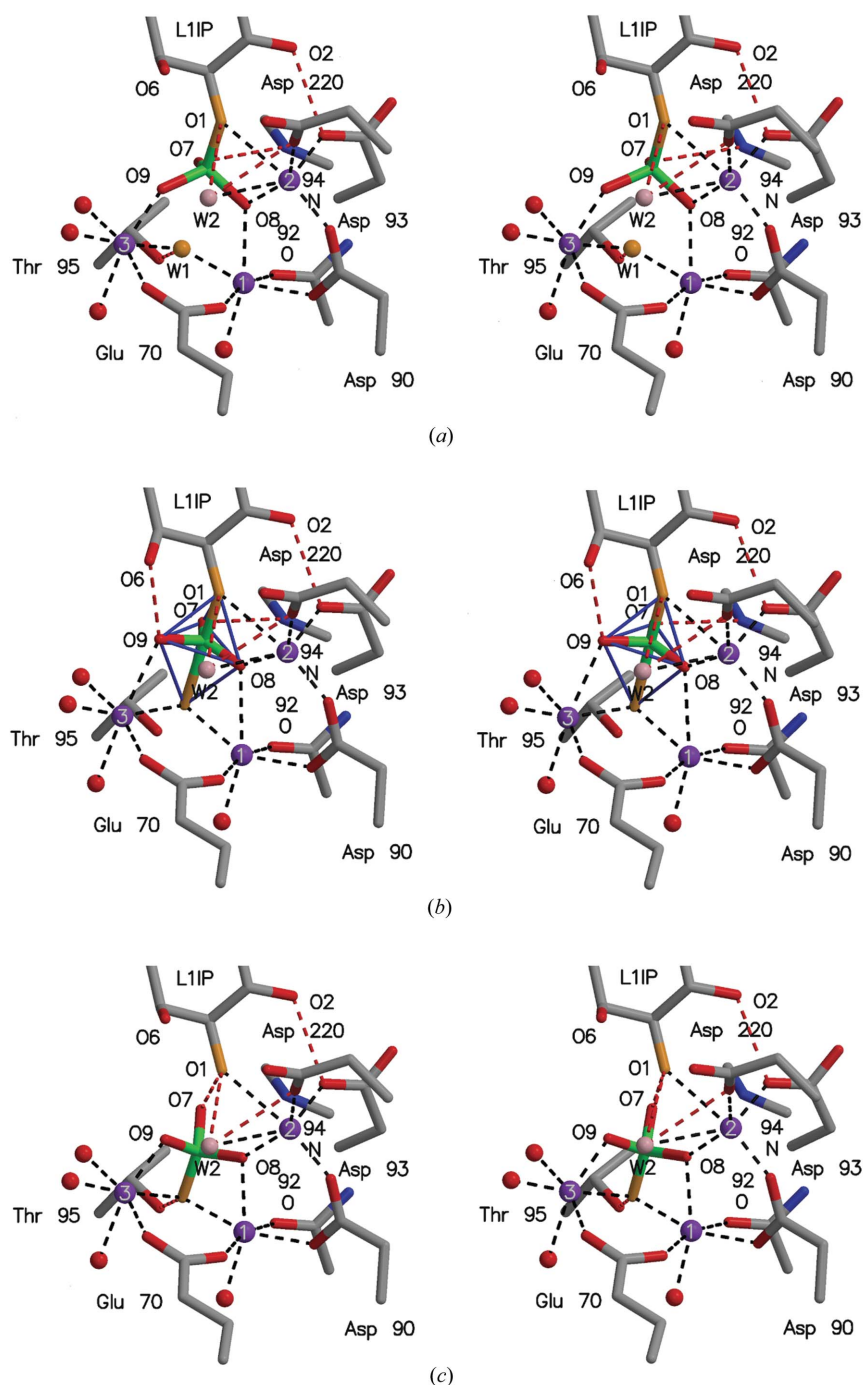
Figure 5
The essential features of the catalytic mechanism of IMPase. (*a*) Modelling of the phosphate moiety of L-Ins(1)P in the pre-reaction state. A slight rotation of the phosphate moiety about O1 superposes the axial phosphate O atoms onto the positions of three active-site waters and orientates the phosphoester bond for a direct inline attack by the putative water nucleophile (W1), which is depicted in orange. Mg-1 and Mg-3 coordinate W1, thus lowering its pK_a and facilitating proton removal by the Thr95/Asp49 dyad. (*b*) Modelling of the trigonal bipyramidal transition state based upon the structure of the pentavalent phosphorus intermediate of phosphorylated β-phosphoglucomutase (Lahiri *et al.*, 2003). The O6 hydroxyl of L-Ins(1)P is within hydrogen-bonding distance of O9 of the phosphate moiety. Whether the species represents a classical transition state as implied here or a trappable pentavalent intermediate is not the focus of the present work. (*c*) Modelling of the post-reaction structure based upon the yeast Hal2p PAPase–3Mg^{2+}–AMP–P$_i$ end-product complex (Patel, Martínez-Ripoll *et al.*, 2000). The collapse of the transition state yields inositolate complexed to Mg-2 and the cleaved phosphate, formed by an inversion of configuration. Inositol is generated through protonation by W2 (depicted in pink) and released as the first product.

Mn-1 and Ca-1 sites identified in human IMPase structures. Similarly, the coordination sphere of Mg^{2+} at site 2 (Mg-2) consists of the conserved residues Asp90, Asp93, Asp220 and three water molecules, one of which is shared with Mg-1. Mg-2 can be directly superposed onto the Mn-2 and Ca-2 sites identified in human IMPase structures. The coordination sphere of Mg^{2+} at site 3 consists of a single protein ligand (Glu70) and five water molecules, one of which is shared with Mg-1. The Mg-3 site can be directly superposed onto the Mn-3 and Ca-3 sites identified in human IMPase structures. The water molecule (W1) shared by Mg-1 and Mg-3 is ideally placed for activation by the Thr95/Asp49 relay and an inline attack on the phosphoester bond of inositol monophosphate. One of the water molecules (W2) coordinated to Mg-2 is weakly bound and hydrogen bonded to Asp220, making it ideally placed for the protonation of the leaving inositol moiety.

3.7. The substrate-binding site of bovine IMPase

The structure of bovine IMPase and the structures of human IMPase–Gd^{3+} in complex with D- and L-Ins(1)P (Bone, Frank, Springer, Pollack *et al.*, 1994) are very similar, with r.m.s. deviations of 0.62 and 0.64 Å, respectively, over 271 equivalent C$_\alpha$ atoms (subunit *A*). The substrate-binding residues Asp93 and Glu213 are conserved between human and bovine IMPase structures and modelling of L-Ins(1)P binding to bovine IMPase demonstrates that four active-site water molecules would be displaced by the three axial phosphate O atoms and O1 of the substrate (Fig. 4). A slight rotation of the phosphate moiety about O1 (r.m.s. deviation 0.49 Å) superposes the axial phosphate O atoms onto these water positions (r.m.s. deviation 0.29 Å) and orientates the phosphoester bond for a direct inline attack by the putative water nucleophile (W1).

In this model, the metal ion at site 3 is not displaced by the phosphate moiety of the substrate, unlike in the crystal structure of human IMPase–Mn^{2+} with phosphate (Bone, Frank, Springer & Atack, 1994). However, the model is consistent with the structure of the human enzyme in complex with D-Ins(1)P and three calcium ions (Ganzhorn & Rondeau, 1997) in which the third metal

ion, like the first metal ion, is also ligated to Glu70 and a phosphate O atom.

3.8. A detailed three-metal mechanism for IMPase

The high resolution structure of bovine IMPase in complex with Mg^{2+}, when combined with the results of earlier functional studies in solution, the structure of human IMPase in complex with L-Ins(1)P (Bone, Frank, Springer, Pollack et al., 1994) and the recently determined structures of the penta-valent phosphorus intermediate of phosphorylated β-phos--phosphoglucomutase (Lahiri et al., 2003) and the lithium-sensitive yeast Hal2p PAPase end-product complex (Patel, Martínez-Ripoll et al., 2002), allows for the formulation of a detailed proposal for the catalytic mechanism.

The high-affinity metal site (site 1; $K_d \simeq 300\ \mu M$) is assumed to be occupied at ambient Mg^{2+} concentration (~ 0.5 mM in cortical neurones; Brocard et al., 1993). Binding of the substrate then promotes the cooperative binding of Mg^{2+} at site 2 ($K_d \simeq 3$ mM in the absence of the phosphate moiety), simultaneously bringing in an Mg^{2+} counterion which binds weakly and non-cooperatively at site 3 (Johnson et al., 2001). By superimposing the structure of the Mg^{2+}-bound bovine enzyme on the L-Ins(1)P–Gd^{3+}–Li^+ human IMPase structure, a plausible model for the arrangement of the reactants prior to the transition state may be deduced (Fig. 5a). Most of the substrate-binding energy is contributed by the phosphate moiety interacting with the active-site metals (Gee et al., 1988). The bridging phosphate oxygen O1 coordinates Mg^{2+}-2 and the non-bridging phosphate oxygen O9 coordinates Mg^{2+}-3, O8 coordinates both Mg^{2+}-1 and Mg^{2+}-2 and O7 hydrogen-bonds to the backbone amide of Ala94. The extensive phosphate–metal coordination neutralizes the negatively charged phosphate O atoms to allow inline attack at the scissile phosphoester bond by the previously identified water nucleophile (W1), which bridges both Mg^{2+}-1 and Mg^{2+}-3. W1 has a very low B factor (11.8 Å^2 compared with the average of 27.1 Å^2, $\delta = 11.5$ Å^2), but in the absence of substrate displays no anisotropy. The activation of W1 is most likely to derive from the transfer of a proton from W1 to Thr95 OG and from this residue to Asp49 OD1 (Patel, Martínez-Ripoll et al., 2002), both of which are conserved among the Li^+-inhibited phosphomonoesterases.

The emerging hydroxide ion at W1 whose pK_a is reduced by the positively charged centres of Mg^{2+}-1 and Mg^{2+}-3 approaches the phosphate in an inline attack. The low-energy negatively charged trigonal bipyr-amidal transition state (Fig. 5b) formed during phosphoryl transfer, with the charge stabilized by Mg^{2+}-2 and the dipoles of helices α_4 (residues 95–101) and α_7 (residues 195–205), would be energetically favoured by symmetrical coordination of the axial ligand to Mg^{2+}-1 and Mg^{2+}-3. Modelling of the pentavalent phosphorus transition state demonstrates stabilization by coordination to each of the three magnesium ions and by hydrogen bonding to the substrate 6-OH group, orientated to a position coincident with an active-site water molecule.

The trigonal bipyramidal intermediate collapses upon proton transfer to the leaving O1 group of inositol from W2, which is held weakly by Mg^{2+}-2 and also hydrogen bonded to Asp220, resulting in phosphate hydrolysis. The post-reaction geometry can be modelled on that of the yeast Hal2p PAPase–$3Mg^{2+}$–AMP–P_i end-product complex (Patel, Martínez-Ripoll et al., 2002; Fig. 5c). The phosphate ion displays inversion of configuration and is transiently bound to all three magnesium ions. The sequence of release of products from the IMPase–$3Mg^{2+}$–L-Ins–P_i end-product complex is not shown in Fig. 5 but presumably the weakly bound metal Mg^{2+}-3 debinds first upon consumption of W1, followed by inositolate after attack by W2 (Miller et al., 2000; Patel, Martínez-Ripoll et al., 2002) and then Mg^{2+}-2, the thermal ellipse of which displays a prominent displacement towards the phosphoester bond, regenerating metal 1-bound enzyme for the next hydrolytic cycle. It has been proposed that the dissociation of Mg^{2+}-2 is hindered at higher Mg^{2+} concentration, trapping the phos-phate and effectively inhibiting the enzyme (Leech et al., 1993; Pollack et al., 1994; Saudek et al., 1996).

3.9. Modelling of the lithium-inhibited IMPase–product complex

The Li^+-inhibited IMPase structure can be modelled on that of the yeast Hal2p PAPase–$2Mg^{2+}$–AMP anion–P_i–Li^+ complex (Albert et al., 2000) in which the tetrahedral co-ordination of Li^+ at site 2 has been inferred (Fig. 6). Since Li^+ coordinates O1 of inositol and O8 of the phosphate moiety in the same manner as Mg^{2+}, it is not clear whether Li^+ itself is capable of promoting hydrolysis or whether it simply displaces Mg^{2+}-2 following phosphoester-bond cleavage and traps the inorganic phosphate and inositolate in the active site.
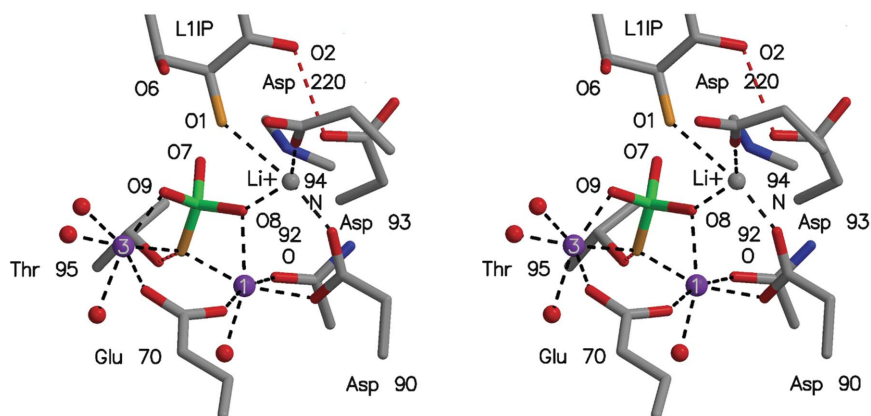

Figure 6
Modelling of the lithium-inhibited IMPase structure based upon that of the yeast Hal2p PAPase–$2Mg^{2+}$–AMP anion–Li^+ complex (Albert et al., 2000), in which the tetrahedral coordination of Li^+ at site 2 has been inferred. Replacement of Mg^{2+}-2 by Li^+-2 precludes the coordination of W2 and prevents the protonation of the inositolate group after phosphoester hydrolysis, trapping inositolate and P_i in the active site and effectively inhibiting the enzyme.

However, the demonstration that IMPase releases inositol from Ins(1)P in a burst faster than the rate of steady-state substrate turnover in the presence of Li$^+$ dictates that inhibition by Li$^+$ is a post-catalytic event following phosphoester bond cleavage (Leech *et al.*, 1993).

4. Discussion

Three Mg^{2+} ions are bound at the active site of each bovine IMPase monomer at positions identical to those occupied by partially activating Mn^{2+} and inhibitory Ca^{2+} ions in human IMPase structures (Bone, Frank, Springer & Atack, 1994; Ganzhorn & Rondeau, 1997). The structural features of the active site of IMPase found in this study are directly superimposable on those of PAPase and PIPase, which both utilize three Mg^{2+} ions for the multiple roles of binding the phosphate ester group, harnessing a water molecule for inline attack, stabilizing the trigonal geometry at the phosphate atom and finally transiently binding the two hydrolysis products for subsequent release (Albert *et al.*, 2000; Patel, Yenush *et al.*, 2002).

The two-metal-ion catalysis proposed for the archael FBPase/IMPases has recently been amended to a three-metal-ion substrate-assisted catalysis (Stec, Johnson *et al.*, 2000; Johnson *et al.*, 2001). In the detailed three-metal mechanism presented here for IMPase, the third metal ion is also carried in by the substrate and although its binding is weak and not cooperative, it is absolutely necessary for the creation of the water nucleophile. Indeed, metals 1 and 3 constitute a classic homobinuclear centre bridged by a bidentate carboxylate (Rardin *et al.*, 1991) and two metal ions have been shown to further lower the pK_a of a coordinated water molecule over the lowering achieved by just one metal ion (Dismukes, 1996; Christianson, 1997). The binuclear centre plays a special role in stabilizing the formation of the trigonal bipyramidal transition state through the symmetric coordination of the incoming and departing anionic fragments and there is ample precedent for nucleophilic metal-bridging water molecules in hydrolytic metalloenzymes (Lipscomb & Sträter, 1996; Christianson & Cox, 1999).

Modelling of the trigonal bipyramidal transition state demonstrates for the first time the role of the 6-OH substrate group in its stabilization and hence lowering of the activation energy. Kinetic studies on both isomers of glycerophosphate and two deoxy forms of β-glycerophosphate demonstrate the importance of both hydroxyl groups flanking the phosphate (Attwood *et al.*, 1988) and studies on substrate-based analogues (Baker *et al.*, 1989, 1990) highlight the necessity for a hydrogen-bond donor at the 6′ position. It has been proposed that the role of the substrate 6-OH group is to hydrogen bond to a water or hydroxide ion located on Mg^{2+}-2 to serve as a proton donor for the inositolate leaving group (Miller *et al.*, 2000). Although the modelled location of the D-Ins(1)P 6-OH group is within hydrogen-bonding distance of W2 (3.0 Å), the 6-OH group of L-Ins(1)P which is a better substrate (Gee *et al.*, 1988) is too distant at 3.8 Å and its role appears to be in direct stabilization of the transition state.

Although X-ray methods are unable to observe Li$^+$ directly, metal site 2 is clearly formed and most likely occupied by Li$^+$ in crystals grown in high concentrations of Li$_2$SO$_4$ (Bone *et al.*, 1992; Bone, Frank, Springer, Pollack *et al.*, 1994; Albert *et al.*, 2000; Patel, Yenush *et al.*, 2002). A nuclear magnetic resonance study of ^{7}Li binding to IMPase provided the first direct evidence of Li$^+$ ion binding to IMPase (Saudek *et al.*, 1996), the dissociation constant of 1.0 mM being in excellent agreement with the kinetic K_i value (Strasser *et al.*, 1995) and consistent with binding at site 2. Remarkably, in contrast to IMPase, the bifunctional archael IMPase/FBPase enzymes are not inhibited by Li$^+$ in the submillimolar range despite possessing a similar Mg^{2+}-coordination geometry at site 2 (Stieglitz *et al.*, 2002). A structural comparison (Stec, Yang *et al.*, 2000; Stieglitz *et al.*, 2002) implicates the conformation of the catalytic loop (β-hairpin residues 32–43) involved in positioning the third metal ion and which has previously been shown to be important for catalysis, transmission of the AMP allosteric signal and inhibition of FBPase (Choe *et al.*, 1998). It has been proposed that Li$^+$ binds at site 3 but that in the three-metal mechanism its smaller charge would be unable to create the water nucleophile, effectively inhibiting the enzyme. Since five of the six Mg^{2+} ligands at site 3 are water molecules, the change from octahedral to tetrahedral coordination could be easily accommodated. In support of this hypothesis, Li$^+$ inhibition of K36Q human IMPase is greatly reduced and noncompetitive and the mutant enzyme is no longer inhibited at high Mg^{2+} concentration (Ganzhorn *et al.*, 1996). However, although the presence of Li$^+$ can be inferred at site 2 in the yeast Hal2p PAPase–2Mg^{2+}–AMP anion–P$_i$–Li$^+$ structure, Mg^{2+} clearly occupies site 3 (Albert *et al.*, 2000). An alternative hypothesis (Chen & Roberts, 1999) highlights the sequence differences between the Li$^+$- and Mg^{2+}-inhibited IMPases and the hyperthermophilic IMPase/FBPases at positions corresponding to residues 217 and 218 in the vicinity of site 2. Clearly, the unequivocal identification of the Li$^+$-binding site must await the determination of the IMPase structure by neutron scattering.

References

Albert, A., Yenush, L., Gil-Mascarell, M. R., Rodriguez, P. L., Patel, S., Martínez-Ripoll, M., Blundell, T. L. & Serrano, R. (2000). *J. Mol. Biol.* **295**, 927–938.

Allison, J. H. & Stewart, M. A. (1971). *Nature New Biol.* **233**, 267–268.

Atack, J. R., Broughton, H. B. & Pollack, S. (1995). *FEBS Lett.* **361**, 1–7.

Attwood, P. V., Ducep, J. B. & Chanal, M. C. (1988). *Biochem. J.* **253**, 387–394.

Baker, G. R. & Gani, D. (1991). *Bioorg. Med. Chem. Lett.* **1**, 193–196.

Baker, R., Carrick, C., Leeson, P. D., Lennon, I. C. & Liverton, N. J. (1991). *J. Chem. Soc., Chem. Commun.*, pp. 298–300.

Baker, R., Kulagowski, J. J., Billington, D. C., Leeson, P. D., Lennon, I. C. & Liverton, N. (1989). *J. Chem. Soc., Chem. Commun.*, pp. 1383–1385.

Baker, R., Leeson, P. D., Liverton, N. J. & Kulagowski, J. J. (1990). *J. Chem. Soc. Chem. Commun.*, pp. 462–464.

Berridge, M. J., Downes, C. P. & Hanley, M. R. (1982). *Biochem. J.* **206**, 587–595.

Bone, R., Frank, L., Springer, J. P. & Atack, J. R. (1994). *Biochemistry*, **33**, 9468–9476.

Bone, R., Frank, L., Springer, J. P., Pollack, S. J., Osborne, S., Atack, J. R., Knowles, M. R., Mcallister, G., Ragan, C. I., Broughton, H. B., Baker, R. & Fletcher, S. R. (1994). *Biochemistry*, **33**, 9460–9467.

Bone, R., Springer, J. P. & Atack, J. R. (1992). *Proc. Natl Acad. Sci. USA*, **89**, 10031–10035.

Brocard, J. B., Rajdev, S. & Reynolds, I. J. (1993). *Neuron*, **11**, 751–757.

Brünger, A. T. (1992). *Nature (London)*, **355**, 472–474.

Brünger, A. T., Adams, P. D., Clore, G. M., DeLano, W. L., Gros, P., Grosse-Kunstleve, R. W., Jiang, J.-S., Kuszewski, J., Nilges, N., Pannu, N. S., Read, R. J., Rice, L. M., Simonson, T. & Warren, G. L. (1998). *Acta Cryst.* D**54**, 905–921.

Chen, I.-W. & Charalampous, F. C. (1966). *J. Biol. Chem.* **241**, 2194–2199.

Chen, L. & Roberts, M. (1999). *Appl. Env. Microbiol.* **65**, 4559–4567.

Choe, Y. Z., Poland, B. W., Fromm, H. J. & Honzatko, R. B. (1998). *Biochemistry*, **37**, 11441–11450.

Christianson, D. W. (1997). *Prog. Biophys. Mol. Biol.* **67**, 217–243.

Christianson, D. W. & Cox, J. D. (1999). *Annu. Rev. Biochem.* **68**, 33–37.

Cole, A. G. & Gani, D. (1994). *J. Chem. Soc. Chem. Commun.*, pp. 1139–1141.

Collaborative Computational Project, Number 4 (1994). *Acta Cryst.* D**50**, 760–763.

Diehl, R. E., Whiting, P., Potter, J., Gee, N., Ragan, C. I., Linemeyer, D., Schoepfer, R., Bennett, C. & Dixon, R. A. F. (1990). *J. Biol. Chem.* **265**, 5946–5949.

Dismukes, G. C. (1996). *Chem. Rev.* **96**, 2909–2926.

Eisenberg, F. Jr (1967). *J. Biol. Chem.* **242**, 1375–1382.

Fauroux, C. M. J., Lee, M., Cullis, P. M., Douglas, K. T., Freeman, S. & Gore, M. G. (1999). *J. Am. Chem. Soc.* **121**, 8385–8386.

Ganzhorn, A. J. & Chanal, M. C. (1990). *Biochemistry*, **29**, 6065–6071.

Ganzhorn, A. J., Hoflack, J., Pelton, P. D., Strasser, F., Chanal, M. C. & Piettre, S. R. (1998). *Bioorg. Med. Chem.* **6**, 1865–1874.

Ganzhorn, A. J., LePage, P., Pelton, P. D., Strasser, F., Vincendon, P. & Rondeau, J.-M. (1996). *Biochemistry*, **35**, 10957–10966.

Ganzhorn, A. J. & Rondeau, J.-M. (1997). *Protein Eng.* **10**(*Suppl.*), 61–70.

Gee, N. S., Ragan, C. I., Watling, K. J., Aspley, S., Jackson, R. G., Reid, G. G., Gani, D. & Shute, J. K. (1988). *Biochem. J.* **249**, 883–889.

Gore, M. G., Greasley, P. J., McAllister, G. & Ragan, C. I. (1993). *Biochem. J.* **296**, 811–815.

Greasley, P. J. & Gore, M. G. (1993). *FEBS Lett.* **331**, 114–118.

Greasley, P. J., Hunt, L. G. & Gore, M. G. (1994). *Eur. J. Biochem.* **222**, 453–460.

Hallcher, L. M. & Sherman, W. R. (1980). *J. Biol. Chem.* **255**, 10896–10901.

Johnson, K. A., Chen, L., Yang, H., Roberts, M. F. & Stec, B. (2001). *Biochemistry*, **40**, 618–630.

Ke, H. M., Thorpe, C. M., Seaton, B. A., Marcus, F. & Lipscomb, W. N. (1989). *Proc. Natl Acad. Sci. USA*, **86**, 1475–1479.

Kraulis, P. J. (1991). *J. Appl. Cryst.* **24**, 946–950.

Lahiri, S. D., Zhang, G., Dunaway-Mariano, D. & Allen, K. N. (2003). *Science*, **299**, 2067–2071.

Laskowski, R. A., McArthur, M. W., Moss, D. S. & Thornton, J. M. (1993). *J. Appl. Cryst.* **26**, 283–291.

Leech, A. P., Baker, G. R., Shute, J. K., Cohen, M. A. & Gani, D. (1993). *Eur. J. Biochem.* **212**, 693–704.

Leslie, A. G. W. (1992). *Jnt CCP4/ESF–EACBM Newsl. Protein Crystallogr.* **26**.

Lipscomb, W. N. & Sträter, N. (1996). *Chem. Rev.* **96**, 2375–2433.

MacLeod, A. M., Baker, R., Hudson, M., James, K., Roe, M. B., Knowles, M. & MacAllister, G. (1992). *Med. Chem. Res.* **2**, 96–101.

Majerus, P. W., Connolly, T. M., Bansal, V. S., Inhorn, R. C., Ross, T. S. & Lips, D. L. (1988). *J. Biol. Chem.* **263**, 3051–3054.

Matthews, B. W. (1968). *J. Mol. Biol.* **33**, 491–497.

Merritt, E. A. & Bacon, D. J. (1997). *Methods Enzymol.* **276**, 505–524.

Miller, D. J., Beaton, M. W., Wilkie, J. & Gani, D. (2000). *Chem. Biochem.* **1**, 262–271.

Navaza, J. (1994). *Acta Cryst.* A**50**, 157–163.

Patel, S., Martínez-Ripoll, M., Blundell, T. L. & Albert, A. (2002). *J. Mol. Biol.* **320**, 1087–1094.

Patel, S., Yenush, L., Rodríguez, P. L., Serrano, R. & Blundell, T. L. (2002). *J. Mol. Biol.* **315**, 677–685.

Pollack, S. J., Atack, J. R., Knowles, M. R., McAllister, G., Ragan, I. C., Baker, R., Fletcher, S. R., Iversen, L. L. & Broughton, H. B. (1994). *Proc. Natl Acad. Sci. USA*, **91**, 5766–5770.

Pollack, S. J., Knowles, R., Broughton, H. B., Ragan, C. I., Osborne, S. A. & McAllister, G. (1993). *Eur. J. Biochem.* **217**, 281–287.

Rardin, R. L., Tolman, W. B. & Lippard, S. J. (1991). *New J. Chem.* **15**, 417–430.

Saudek, V., Vincendon, P., Do, Q.-T., Atkinson, R. A., Sklenár, V., Pelton, P. D., Piriou, F. & Ganzhon, A. J. (1996). *Eur. J. Biochem.* **240**, 288–291.

Sheldrick, G. M. & Schneider, T. R. (1997). *Methods Enzymol.* **277**, 319–343.

Shute, J. K., Gani, D., Baker, R. & Billington, D. C. (1988). *J. Chem. Soc., Chem. Commun.*, pp. 626–628.

Stec, B., Johnson, K. A., Chen, L., Yang, H. & Roberts, M. F. (2000). *Trans. Am. Crystallogr. Assoc.* **35**, 49–63.

Stec, B., Yang, H., Johnson, K. A., Chen, L. & Roberts, M. F. (2000). *Nature Struct. Biol.* **7**, 1046–1050.

Stieglitz, K. A., Johnson, K. A., Yang, H., Roberts, M. F., Seaton, B. A., Head, J. F. & Stec, B. (2002). *J. Biol. Chem.* **277**, 22863–22874.

Strasser, F., Pelton, P. D. & Ganzhorn, A. J. (1995). *Biochem. J.* **307**, 585–593.

Takimoto, K., Okada, M., Matsuda, Y. & Nakagawa, H. (1985). *Biochem. J. (Tokyo)*, **98**, 363–370.

Villeret, V., Huang, S., Fromm, H. J. & Lipscomb, W. N. (1995). *Proc. Natl Acad. Sci. USA*, **92**, 8916–8920.

Wang, D., Driessen, H. P. C. & Tickle, I. J. (1991). *J. Mol. Graph.* **9**, 50–52.

Wilkie, J., Cole, A. G. & Gani, D. (1995). *J. Chem. Soc. Perkin Trans. 1*, **21**, 2709–2727.

York, J. D., Ponder, J. W., Chen, Z. W., Matthews, F. S. & Majerus, P. W. (1994). *Biochemistry*, **33**, 13164–13171.

Zhang, Y., Liang, J.-Y., Huang, S., Ke, H. & Lipscomb, W. N. (1993). *Biochemistry*, **32**, 1844–1857.